Optical Characterization of Lead-Free Cs_2SnI_6 Double Perovskite fabricated from Degraded and Reconstructed $CsSnI_3$ films

Eduardo López-Fraguas,[1,2] Sofia Masi,[1,*] Iván Mora-Seró[1,*]

[1] *Institute of Advanced Materials (INAM) Universitat Jaume I Av. Sos Baynat, s/n, 12071 Castelló, Spain*
[2] *Displays and Photonic Applications Group (GDAF-UC3M), Universidad Carlos III de Madrid, Av. Universidad 30, 28911 Leganés (Madrid), Spain.*

Corresponding Authors: masi@uji.es, sero@uji.es
ORCID: Eduardo López-Fraguas, 0000-0002-7943-4471; Sofia Masi, 0000-0002-7373-1627; Iván Mora-Seró 0000-0003-2508-0994.

Abstract

Halide perovskites have experienced a huge development in the past years, but they still have two major challenges for their massive implantation: the long-term stability and the use of lead. One of the most obvious lead-free candidates to replace these perovskites is $CsSnI_3$ but, due to its poor environmental stability, it has been discarded for the fabrication of stable devices. Nevertheless, ambient degradation of $CsSnI_3$ and ulterior reconstruction produces relatively stable lead-free Cs_2SnI_6 double perovskite with interesting optical properties that have not been deeply characterized previously. In this work, the potentiality of the optical properties of Cs_2SnI_6 is studied and compared with the most common halide perovskite, $CH_3NH_3PbI_3$ ($MAPbI_3$). The Cs_2SnI_6 films stayed in standard atmosphere during a week without showing any signs of degradation. They also demonstrated better reflective behavior than $MAPbI_3$ and higher absorption in the 650 nm and 730 nm spectral range, making this material interesting for the development of photodetectors in this region. This study demonstrates that Cs_2SnI_6 is a promising material for photo-devices, as it highlights its main characteristics and optical parameters, giving an original view on the use of the double perovskite, but at the same time emphasizing the need to improve the electrical properties for the development of efficient optoelectronic devices.

Keywords: Optical characterization, lead-free, perovskite, co-evaporation deposition, tin-halide, full inorganic.

Introduction

Lead halide perovskites ($APbX_3$, being A, an organic/inorganic cation and X an halide anion) have experienced a huge development in the past years, due to their suitability in the fabrication of solar cells, going from an initial 3.81% power conversion efficiency[1] to the recently achieved 25.2%.[2] These perovskites have demonstrated their great absorption capabilities, high photoluminescence quantum yield and cheap

fabrication processes. All these facts make them great candidates not only for the solar cell world, but also for other optoelectronic applications such as solid light emitting,[3, 4] or as photodetectors.[5,6,7] However, these systems present a significant drawback facing their commercialization due to the toxicity of the lead. Consequently, a lot of studies focus on the development of lead-free perovskite with similar characteristics as their lead counterparts. [8,9,10,11]

There are a lot of possible lead-free candidates.[12] However tin halide perovskites have drawn the attention of the scientific community, due to their similarities with the lead halide perovskites.[13, 14] In particular, the fully inorganic $CsSnI_3$ achieved 0.88% of efficiency in its first approach of a Schottky solar cell.[15] Chung et al. studied the electrical properties of $CsSnI_3$, discussing its metallic behavior instead of a semiconductor one.[16] They argued that this behavior is due to the tin vacancies produced in the structure during its formation [17,18,19]. Following that, Marshall et al. included a 10% excess of SnI_2 in the formation of the film, or the 20% of SnF_2[20] to cover the tin vacancies, achieving an efficiency around 2-2.76%.[21,22]

The main drawback of this perovskite is the poor stability in environmental conditions, because the Sn^{2+} is easily oxidized to Sn^{4+}. Lee et al. tried to avoid this oxidation using SnF_2 as a reducing agent in the formation of the formamidinium tin iodide ($FASnI_3$) perovskite, achieving a power conversion efficiency of 4.8%.[23] Recently, Chen et al. mixed the $CsSnI_3$ with germanium (Ge), making a "double perovskite" (Cs_2SnGeI_6) with 7.11% of efficiency.[24] However, the majority of these studies were carried under nitrogen atmosphere. Under these conditions, Sn^{4+} arises, transforming $CsSnI_3$ perovskite into Cs_2SnI_6 double perovskite. Nevertheless, this material itself constitutes a more air stable candidate than its non-oxidized counterpart.[25] It has been previously used as a hole transport layer (HTL) in dye-sensitized solar cells,[26,27,28] and also used as nanowires[29] or quantum rods.[30] Several synthesis methods have been employed for its preparation.[25,31,32] However, the optical properties of this material have not been broadly studied in the literature. In this work, the optical properties of the Cs_2SnI_6, obtained as final degradation product of the $CsSnI_3$ in air, are studied in depth. In order to compare the properties of the thin film material and of the bulk, the powder is also synthesized with a novel and easy precipitation method. Moreover, a comparative analysis of the Cs_2SnI_6 and of the widely used perovskite, the methylammonium lead iodide ($MAPbI_3$) properties, shows the potentiality of the Cs_2SnI_6 not only in terms of ambient stability but also from the optical point of view. With this study, we intend to pave the way to further electric studies of this promising lead-free material, facing the fabrication of efficient optoelectronic devices.

Experimental section

Thin film fabrication: $CsSnI_3$ thin film was deposited using a co-evaporation technique, as can be schematically seen in Figure 1. We used a MBraun Thermal Evaporator, filling two crucibles with the precursors: one with CsI (99.9%, Sigma Aldrich), and the other one with SnI_2 (99.9%, Sigma Aldrich). The glass substrates were previously cleaned with soap water ultrasonic bath, rinsed with MiliQ water, ultrasonicated with ethanol and isopropanol (1:1) and then ultrasonicated again with ethanol and acetone (1:1).

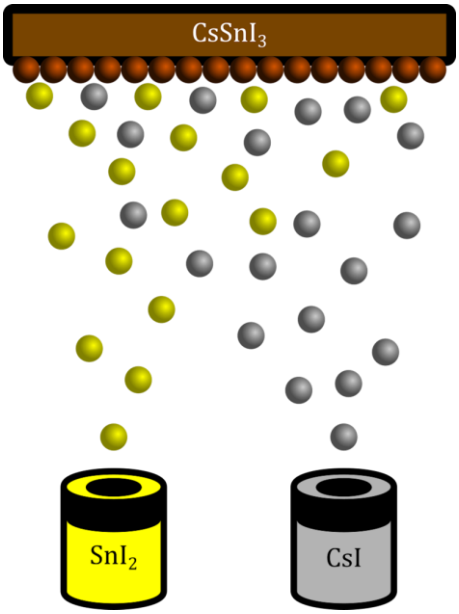

Figure 1. Scheme of the thermal co-evaporation fabrication process for the preparation of $CsSnI_3$.

The co-evaporation of the binary salts leads to the self-assembly of the two precursors and to the formation of the lead-free perovskite (Equation 1):

$$1CsI + 1SnI_2 \rightarrow CsSnI_3 \quad (1)$$

The co-evaporation process involved heating the two crucibles simultaneously under vacuum, then the sublimation until the desired deposition rate was reached for both precursors.

In order to achieve the correct stoichiometry (1:1) in the final film, it is convenient to calculate the deposition rate ratio. It is, in fact, reasonable that the material volume ratio is proportional to the film thickness, and in turn to the evaporation rate. Thus, the volume ratio, depending on the molecular weight and densities (Equation 2) is equal to the rate ratio.

$$\frac{1\ mol\ CsI}{1\ mol\ SnI_2} \rightarrow \frac{259.81\ g\ CsI}{372.52\ g\ SnI_2} \rightarrow \frac{57.61\ mL\ CsI}{49\ mL\ SnI_2} = \frac{DepositionRate_{CsI}}{DepositionRate_{SnI_2}} = 1.176 \quad (2)$$

This means that, to achieve the correct stoichiometry, the deposition rate of CsI must be 1.176 times bigger than the one of SnI_2. With this simple calculation, we can customize the ratio between the two precursors, and make films with CsI or SnI_2 excess, having different properties. [22,33] The optimized temperature values for each crucible are: ~270°C for SnI_2 and ~510°C for CsI. All these co-evaporations took place with the evaporator at $3x10^{-6}$ Torr pressure, inside a nitrogen filled glove-box.

Reconstruction conditions: The conversions to Cs_2SnI_6 were carried in dark, with a temperature between 21 °C and 23 °C and relative humidity of 28-35%. The samples were stored in aluminium wrapped boxes in laboratory conditions, in air.

Cs_2SnI_6 powder synthesis: pure powder of Cs_2SnI_6 was synthesized with the following procedure. 1 mmol of CsI (259.81 mg) was mixed with 1 mmol of SnI_2 (372.52 mg) in a vial. 1mL of acetone was added to the mixture to form a black suspension, gently

stirred at 750 rpm for a couple of hours, in order to completely disperse the precursors. After the evaporation of the acetone in ambient conditions it was possible to collect the precipitated black crystals of Cs_2SnI_6.

Materials characterization: X-Ray Diffraction (XRD) measurements of the powders and the thin films were taken by an X-Ray diffractometer (D8 Advance, Bruker-AXS) (Cu Kα, wavelength $\lambda = 1.5406$ Å). UV-VIS spectrophotometer (Cary 300 UV-VIS, Agilent) was used to measure the absorbance, reflectance and transmittance of the films. Photoluminescence (PL) measurements were done using a spectrofluorometer (Fluorolog, Horiba). The Photoluminescence Quantum Yield (PLQY) measurement was taken using an integrating sphere (Hamamatsu). Thicknesses of the films were obtained using a profilometer (Dektak 6M, Veeco). All the microscopy was done using a Scanning Electron Microscope (SEM) (JSM-7001F, JEOL) which was equipped with Energy Dispersive X-Ray Spectroscopy (EDS) too.

Results and Discussion

$CsSnI_3$ prepared on glass substrate by co-evaporation (see Experimental section) inside the glovebox were characterize in ambient conditions. After 10 minutes of ambient air exposure, samples experienced a fast degradation in their precursors (Figure 2a) with a decrease of the absorbance (Figure 2b). Accordingly, their color changed from dark brown ($CsSnI_3$, left) to yellow (CsI + SnI_2, center). The poor stability of the $CsSnI_3$ in air is mainly due to the decomposition (Equation 3) and oxidation (Equation 4) mechanisms.

$$CsSnI_3 + Environmental\ conditions \rightarrow CsI + SnI_2 \quad (3)$$

$$2SnI_2 + O_2 \rightarrow SnI_4 + SnO_2 \quad (4)$$

The oxidation from Sn^{+2} to Sn^{+4} leads to the phase conversion to Cs_2SnI_6, in which half of the tin atoms are missed, because they form tin oxide. The complete reaction is shown in Equation 5.

$$2CsSnI_3 + O_2 \rightarrow Cs_2SnI_6 + SnO_2 \quad (5)$$

This $CsSnI_3$ degradation and Cs_2SnI_6 reconstruction has been demonstrated by Qiu et al. [34] but with some differences. In our case, the degradation and reconstruction take between 3 and 5 days to get the film completely dark (Figure 2a, right) against the 24h taken in that study. This enhanced stability of initial $CsSnI_3$ is attributed to better quality of the deposition method here employed, as they reported a two-step sequential deposition by alternating thermal evaporation depositions, followed by a thermal annealing to provoke a solid-state reaction between the layers. This method increases the chance of getting pin-holes and an inhomogeneous morphology, compared to the film obtained by thermal co-evaporation.[34] The absorbance spectra reported in Figure 2c show that the film recovers its capacity to absorb the wavelengths between 700 nm and 800 nm completely, but losing the absorption capacity in shorter wavelengths, and having a planar response with two humps, instead of the original ramp shape. This characteristic behavior, resulting in an average

visible transmittance (AVT) of 42.1%, doubling the value of the AVT reported for 150 nm MAPI films,[35,36] is attractive for semitransparent application.[37] In this case the thickness, measured using a profilometer and by SEM cross section, giving a result of 230 nm (Figure S1a,b) was not sacrificed to obtain a high transmittance value, avoiding the problems related to the contact between the deposited layer above and below the perovskite, leading to short circuit in optoelectronic devices. Note that slower degradation of $CsSnI_3$ is observed in the inferior side of the analyzed sample, Figure 2a, where FTO (Fluorine doped SnO_2) is exposed in the substrate. This fact points to a possible effect of fluorine in FTO as a reducing agent[23] in the enhanced stability of $CsSnI_3$ in this region. However, deep analysis of this observation is beyond the scope of this work.

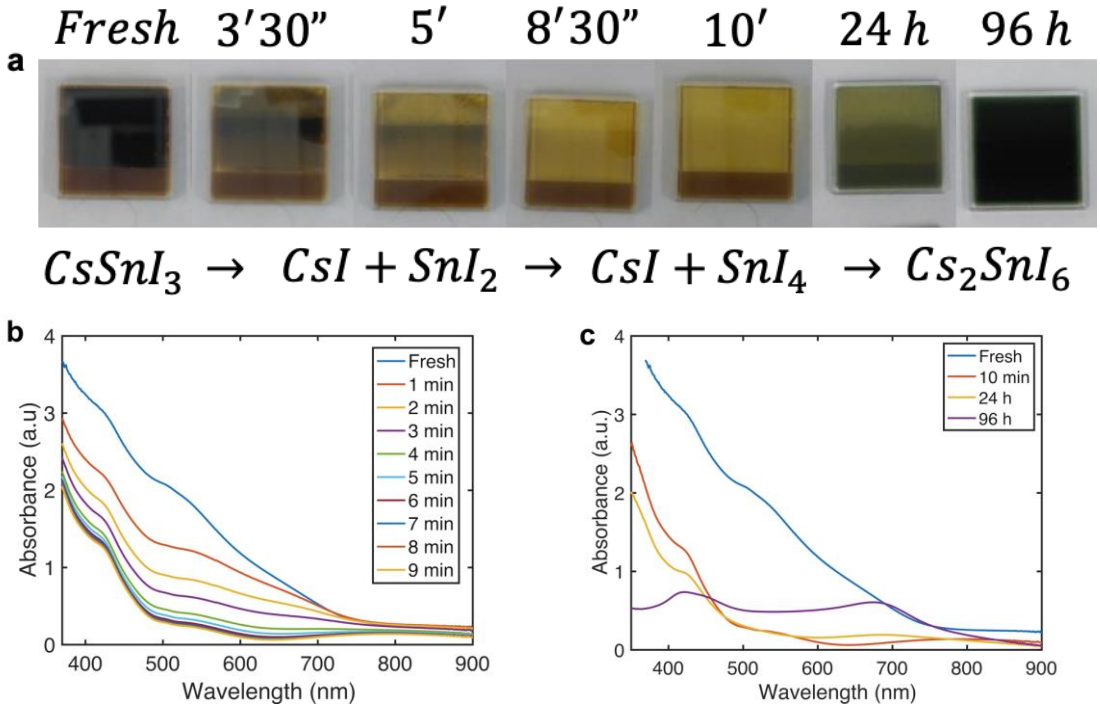

Figure 2. a) Degradation, oxidation of $CsSnI_3$ and reconstruction of the Cs_2SnI_6 thin film. b) Absorbance decay due to $CsSnI_3$ degradation. c) Absorbance recovery due to formation of Cs_2SnI_6.

To compare the properties in bulk, we synthesized the Cs_2SnI_6 powder following the procedure explained in the Experimental Section. The X-Ray Diffraction (XRD) patterns of the powder and of the thin film are shown in Figure 3a. Here, we considered the powder (Figure 3b) as a reference pure material, with characteristic peaks at 13.16°, 26.52°, 30.72°, 44°, 52.04° and 54.68°, all of them representing lattice planes of Cs_2SnI_6.[26,32,33] After comparing these peaks with a film exposed to ambient air for five days, it is possible to recognize similar patterns in the degraded and reconstructed samples. However, three days after, another two peaks have arisen, at 27.6° and 48.76°, both belonging to CsI, one of the precursors. This fact implies that the films maintain their air stability for one week, approximately. Then, they start decomposing in their precursors again. This points out that despite Cs_2SnI_6 double perovskite presents an enhanced stability compared with most of its perovskite counterparts also requires encapsulation for long term stability.

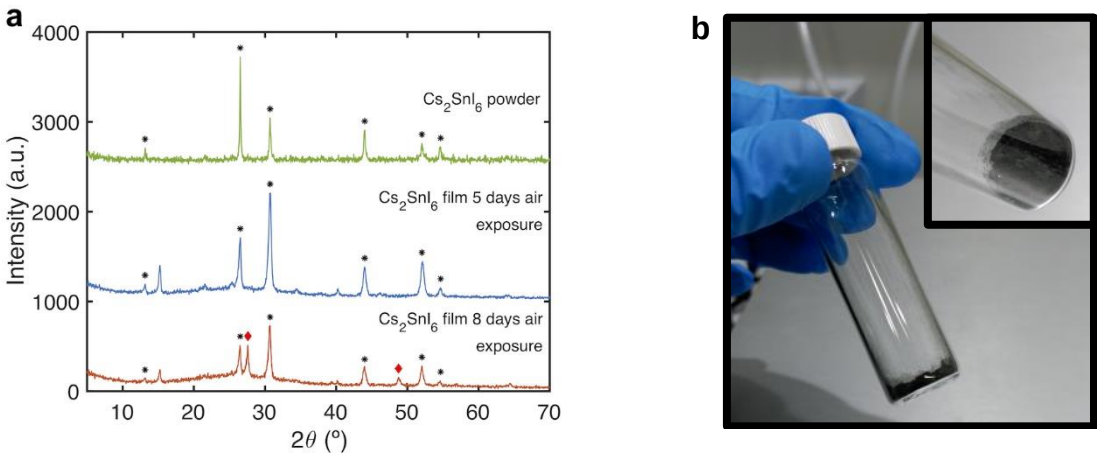

Figure 3. a) XRD patterns of the pure powder and the thin-films of $CsSnI_3$ after 5 days and 8 days in air. After 5th day the $CsSnI_3$ film is totally converted in the Cs_2SnI_6. Black stars show Cs_2SnI_6 peaks, and red diamonds show the CsI peaks. b) Picture of the Cs_2SnI_6 pure powder.

To double-check the presence of the CsI, we measured the morphology by Scanning Electron Microsopy (SEM) (Figure 4). The pure powder presents crystals with tiny bright dots in secondary electrons image, but not in backscattered one. In fact, the crystal and the bright dots were analyzed using Energy-Dispersive X-Ray Spectroscopy (EDS) measurements, giving both the same result, Cs≈22%, Sn≈11% and I≈66%, matching with Cs_2SnI_6 structure (Figure S2a). Figure 4b shows that the surface of the thin-film before the final decomposition is rough. Although it was not possible to measure the $CsSnI_3$ film, because of the fast degradation, we are confident that the morphology is homogeneous, as the co-evaporation give a perfect mirror-like film (Figure S3). Consequently, the roughness observed in the Cs_2SnI_6 is likely generated during the oxidation and reconstruction process, as briefly mention above.

In Figure 4c and 4d we can see the surface of the Cs_2SnI_6 thin-film starting the degradation process, because crystals of CsI start appearing. The composition of the crystals was confirmed by EDS measurements (Figure S2b).

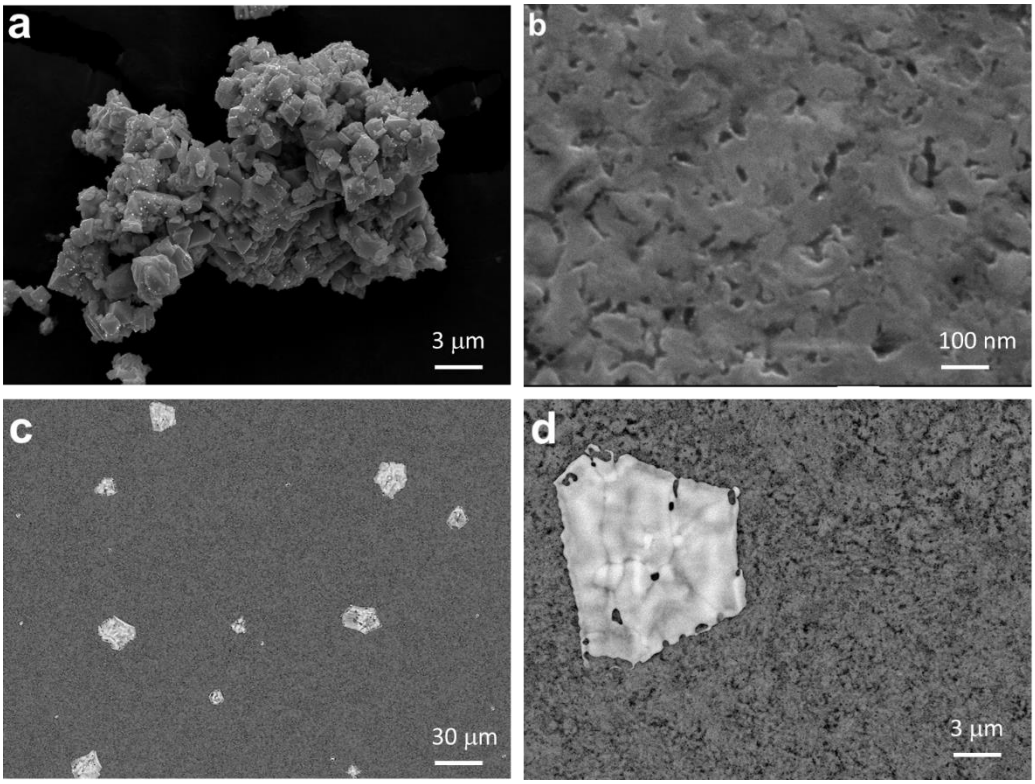

Figure 4. Scanning Electron Microscopy (SEM) images of a) pure powder sample; b) Cs2SnI6 samples. c) After 11 days on the SEM top view of the Cs_2SnI_6 CsI crystals became visible. d) Zoom-in of the CsI crystal detail.

Optical properties of the Cs_2SnI_6 thin films prepared by degradation and reconstruction were systematically analyzed. We measured and calculated the absorption coefficient, band-gap, refractive index and extinction coefficient.

The absorption, reflection and transmission of the films were measured, (Figure 5a) and the corresponding values were used to obtain the absorption coefficient, α, using the relation below: [38]

$$\alpha = \frac{1}{t} \cdot \ln\left[\frac{(1-R)^2}{T}\right] \approx 2.303 \cdot \frac{A}{t} \tag{6}$$

where, t is the thickness of the film, and R, T, A are Reflectance, Transmittance and Absorbance of the film. The approximation showed in Equation 6 is accepted if the reflectance is close to zero. In this study, the approximation matches the real case, due to the low reflection of the film (Figure 5a).

The values of refractive index and extinction coefficient as a function of wavelength, see Figure 5b, were obtained following Equation 7 and 8:[38]

$$\kappa = \frac{\alpha\lambda}{4\pi} \tag{7}$$

$$n = \frac{-2(R+1) \pm \sqrt{\left(2(R+1)\right)^2 - 4(R-1)^2(1+\kappa^2)}}{2(R-1)} \tag{8}$$

where λ is the wavelength, R is the measured reflectance, n is the refractive index and κ the extinction coefficient.

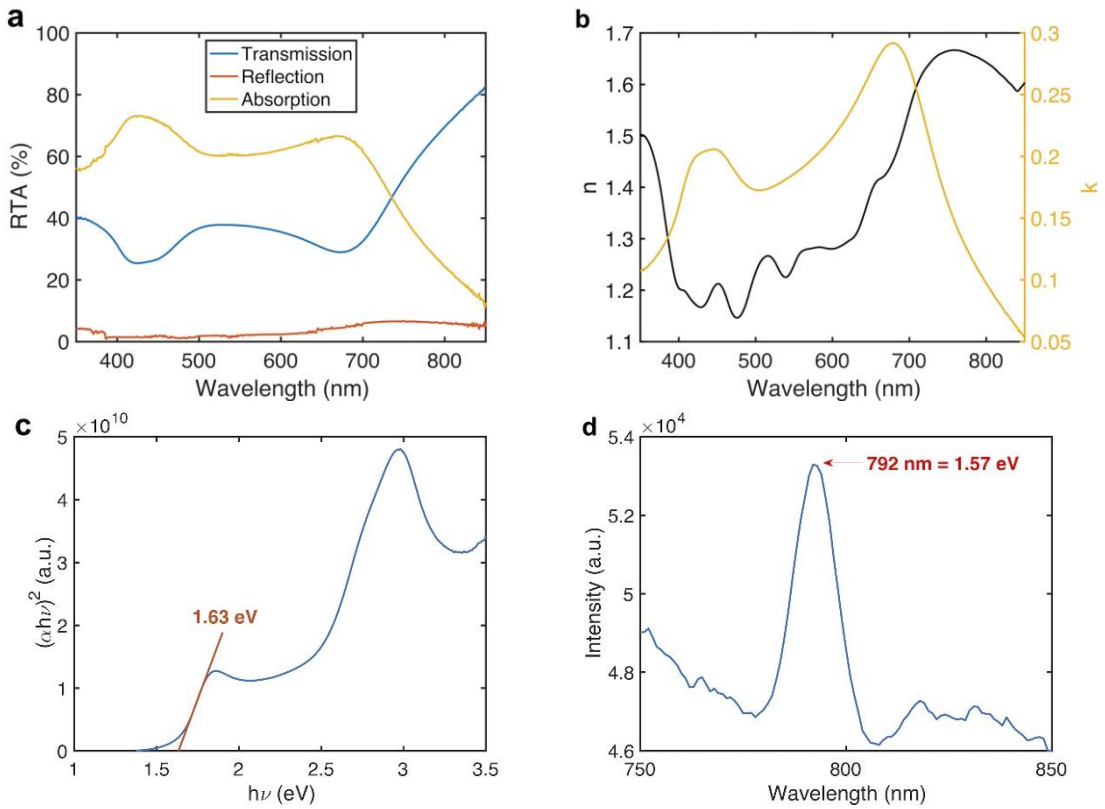

Figure 5. Optical characterization of Cs_2SnI_6 thin films a) Reflection, Transmission and Absorption measurements. b) Refractive index and extinction coefficient values. c) Tauc plot determines the band-gap. d) The photoluminescence peak matches with the band-gap.

Cs_2SnI_6 thin films presented a bandgap of 1.63 eV, see Figure 5c, as it was calculated using the linear interpolation of the Tauc plot. This plot compares $(\alpha h\nu)^n$ ($n = 2$, considering Cs_2SnI_6 as a direct band-gap material), against the energy of the photons $(h\nu)$, where h is the Planck's constant and ν the photon's frequency. Previous literature provides a wide range of bandgap values for Cs_2SnI_6, between 1.2 to 1.6 eV.[25,26,27,28,32,34] Our work is in good agreement with those pointing to high bandgap in this range.[25,27,32,34] Regarding the optical bandgap, the photoluminescence (PL) of the thin films results in the emission peak (Figure 5d) at 792 nm. Translated to energy, this value means 1.57 eV, which matches with the result obtained from the Tauc plot, with a relatively small Stokes shift. No significant PL quantum yield was measured for this samples, pointing to a high non-radiative recombination of the material.

In order to put this material in context with other materials of the perovskite family, we compared it with the most studied perovskite, $MAPbI_3$.[39] Figure 6a and 6b show the comparison of refractive index and extinction coefficient between both materials. Two main aspects are remarkable here: the first one, regarding to n, is the huge difference between the $MAPbI_3$ (around 2.5) and the Cs_2SnI_6 (around 1.5). This fact can make Cs_2SnI_6 better than $MAPbI_3$ in terms of reflection and interface index matching, depending of the surrounding layers. The second important fact is regarding to κ, as $MAPbI_3$ can be considered a better absorber than Cs_2SnI_6, nevertheless, between 650

nm and 730 nm, Cs_2SnI_6 has a higher extinction coefficient that $MAPbI_3$, which implies that is a better absorber in this spectral interval. This fact points to a high potentiality of Cs_2SnI_6 for the development of photodetectors in this range.

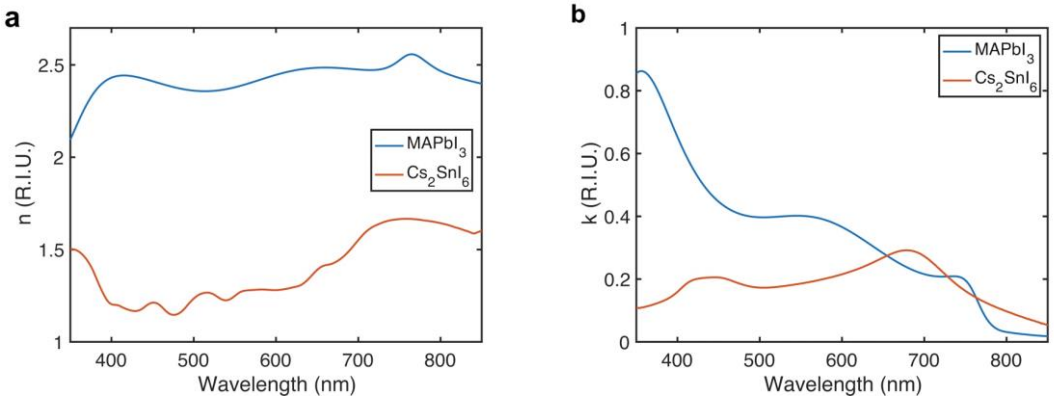

Figure 6. a) Refractive index and b) extinction coefficient comparison between classical $MAPbI_3$ and lead-free (Cs_2SnI_6) perovskite.

With these results it is also possible to calculate the ideal short-circuit current density that a solar cell made with Cs_2SnI_6 could have. We have done this using the generation rate and supposing an ideal case with no electrical losses.[40]

$$J_{SC} = q \cdot \int_0^T G(x) \cdot dx$$

$$J_{SC} = q \cdot \int_0^T \int_{\lambda_{min}}^{\lambda_{max}} \frac{\lambda}{hc} \cdot Irr(\lambda) \cdot [1 - r(\lambda)] \cdot \alpha(\lambda) \cdot e^{-\alpha(\lambda) \cdot x} \cdot d\lambda \cdot dx$$

$$J_{SC} = \frac{q}{hc} \int_{\lambda_{min}}^{\lambda_{max}} \lambda \cdot Irr(\lambda) \cdot [1 - r(\lambda)] \cdot (1 - e^{-\alpha(\lambda) \cdot T}) \cdot d\lambda$$

Being q the electron charge, G(x) the generation rate, h the Planck's constant, c the speed of light, λ the incident wavelength in vacuum, α the absorption coefficient, T the thickness of the film, r the reflectance and Irr the irradiance value of the incident light.

Using this equations, under the Sun spectrum (AM1.5G), we obtain a J_{SC} value of 18.86 mA/cm^2 in a device with an active layer thickness of 230 nm. The maximum value is obtained supposing ideal conditions (zero reflectance and an optimum optical thickness), and equals to 33.68 mA/cm^2. So, making thicker devices, will give us higher current density values (e.g. 26.01 mA/cm^2 @ 500 nm thickness). In thicker cases, several problems start appearing, due to the increase in the distance that the carriers have to travel to reach the electrodes. Nevertheless, these electrical issues are far away from our actual study.

Conclusions

In summary, we have prepared Cs_2SnI_6 thin film from the degradation and reconstruction of $CsSnI_3$ first prepared by co-evaporation. The structural properties of

the Cs_2SnI_6 samples were compared with Cs_2SnI_6 powders, prepared by a novel method, obtaining a good agreement. Cs_2SnI_6 thin films exposed to ambient standard conditions of oxygen and moisture do not exhibit degradation for one week. We have successfully characterized the powder and films obtaining their crystalline structure, band-gap, morphology, and their optical properties (PL, absorption coefficient, band gap, refractive index and extinction coefficient). These values have been compared with $MAPbI_3$ perovskite, unveiling that Cs_2SnI_6 presents better reflective properties than $MAPbI_3$. In addition, despite $MAPbI_3$ presents higher absorption than Cs_2SnI_6 in most of the visible wavelength range, this is not the case in the spectral range between 650 nm and 730 nm, where Cs_2SnI_6 presents higher light absorption, making this material interesting for the development of photodetectors in this specific range or for semitransparent applications. Further research will be needed to improve the electrical properties of this material limited by the high non-radiative recombination as we confirm by PL characterization. All these facts make this lead-free double perovskite, Cs_2SnI_6, a great candidate to be an absorber for photo-devices from an optical point of view and stress the need of further work in the improvement of the electrical properties.

Supporting Information

Scanning Electron Microscopy cross section, Energy-Dispersive X-Ray Spectroscopy, and pictures of the evaporated films are supplied as Supporting Information.

Acknowledgements

E.L.F. wants to express his gratitude to the Ministerio de Educación y Formación Profesional for his doctoral grant (FPU research fellowship FPU17/00612) and his research stay grant (EST18/00399). This work was partially supported by the European Research Council (ERC) via Consolidator Grant (724424 - No-LIMIT) and the European Commission via FET Open Grant (862656 - DROP-IT). We acknowledge SCIC from Jaume I university (UJI) for the help with XRD and SEM-EDS characterization.

References

(1) Kojima, A.; Teshima, K.; Shirai, Y.; Miyasaka, T. Organometal Halide Perovskites as Visible-Light Sensitizers for Photovoltaic Cells. *J. Am. Chem. Soc.* **2009**, 131, 6050-6051.

(2) Dissado, L. A.; Nigmatullin, R. R.; Hill, R. M. The Fading of Memory During the Regresion of Structural Fluctuations. *Adv. Chem. Phys.* **1985**, 63, 253.

(3) Wang, J.; Wang, N.; Jin, Y.; Si, J.; Tan, Z.-K.; Du, H.; Cheng, L.; Dai, X.; Bai, S.; He, H.; Ye, Z.; Lai, M. L.; Friend, R. H.; Huang, W. Interfacial Control Toward Efficient and Low-Voltage Perovskite Light-Emitting Diodes. *Adv. Mater.* **2015**, 27, 2311-2316.

(4) Fakharuddin, A.; Shabbir, U.; Qiu, W.; Iqbal, T.; Sultan, M.; Heremans, P.; Schmidt-Mende, L. Inorganic and Layered Perovskites for Optoelectronic Devices. *Adv. Mater.* **2019**, 0, 1807095.

(5) López-Fraguas, E.; Arredondo, B.; Vega-Colado, C.; Pozo, G. d.; Najafi, M.; Martín-Martín, D.; Galagan, Y.; Sánchez-Pena, J. M.; Vergaz, R.; Romero, B. Visible Light Communication System Using an Organic Emitter and a Perovskite Photodetector. *Org. Electron.* **2019**, 73, 292-298.

(6) Suárez, I.; Hassanabadi, E.; Maulu, A.; Carlino, N.; Maestri, C. A.; Latifi, M.; Bettotti, P.; Mora-Seró, I.; Martínez-Pastor, J. P. Integrated Optical Amplifier–Photodetector on a Wearable Nanocellulose Substrate. *Adv. Opt. Mater.* **2018**, 6, 1800201.

(7) Miao, J.; Zhang, F. Recent Progress on Highly Sensitive Perovskite Photodetectors. *J. Mater. Chem. C* **2019**, 7, 1741-1791.

(8) Chatterjee, S.; Pal, A. J. Influence of Metal Substitution on Hybrid Halide Perovskites: Towards Lead-Free Perovskite Solar Cells. *J. Mater. Chem. A* **2018**, 6, 3793-3823.

(9) Sani, F.; Shafie, S.; Lim, H. N.; Musa, A. O. Advancement on Lead-Free Organic-Inorganic Halide Perovskite Solar Cells: A Review. *Materials (Basel)* **2018**, 11(6), 1008.

(10) Wang, X.; Zhang, T.; Lou, Y.; Zhao, Y. All-Inorganic Lead-Free Perovskites for Optoelectronic Applications. *Mater. Chem. Front.* **2019**, 3, 365-375.

(11) Fu, H. Review of Lead-Free Halide Perovskites as Light-Absorbers for Photovoltaic Applications: From Materials to Solar Cells. *Sol. Energy Mater. Sol. Cells* **2019**, 193, 107-132.

(12) Travis, W.; Glover, E. N. K.; Bronstein, H.; Scanlon, D. O.; Palgrave, R. G. On the Application of the Tolerance Factor to Inorganic and Hybrid Halide Perovskites: a Revised System. *Chem. Sci.* **2016**, 7, 4548-4556.

(13) Konstantakou, M.; Stergiopoulos, T. A Critical Review on Tin Halide Perovskite Solar Cells. *J. Mater. Chem. A* **2017**, 5, 11518-11549.

(14) Shum, K.; Chen, Z.; Qureshi, J.; Yu, C.; Wang, J. J.; Pfenninger, W.; Vockic, N.; Midgley, J.; Kenney, J. T. Synthesis and Characterization of CsSnI3 Thin Films. *Appl. Phys. Lett.* **2010**, 96 (22), 221903.

(15) Chen, Z.; Wang, J. J.; Ren, Y.; Yu, C.; Shum, K. Schottky Solar Cells Based on CsSnI3 Thin-Films. *Appl. Phys. Lett.* **2012**, 101, 093901.

(16) Chung, I.; Song, J. H.; Im, J.; Androulakis, J.; Malliakas, C. D.; Li, H.; Freeman, A. J.; Kenney, J. T.; Kanatzidis, M. G. CsSnI3: Semiconductor or Metal? High Electrical Conductivity and Strong Near-Infrared Photoluminescence from a Single Material. High Hole Mobility and Phase-Transitions. *J. Am. Chem. Soc.* **2012**, 134, 8579-87.

(17) Xiao, Z.; Zhou, Y.; Hosono, H.; Kamiya, T. Intrinsic Defects in a Photovoltaic Perovskite Variant Cs2SnI6. *Phys. Chem. Chem. Phys.* **2015**, 17, 18900-3.

(18) Maughan, A.E.; Ganose, A.M.; Scanlon, D.O.; Neilson, J.R. Perspectives and Design Principles of Vacancy-Ordered Double Perovskite Halide Semiconductors. *Chem. Mater.* **2019**, 31, 1184-1195.

(19) Bounos, G.; Karnachoriti, M.; Kontos, A.G.; Stoumpos, C.C.; Tsetseris, L.; Kaltzoglou, A.; Guo, X.; Lü, X.; Raptis, Y.S.; Kanatzidis, M.G.; Falaras, P. Defect Perovskites under Pressure: Structural Evolution of Cs_2SnX_6 (X = Cl, Br, I). *J. Phys. Chem. C.* **2018**, 122, 42, 24004-24013.

(20) Kumar, M. H.; Dharani, S.; Leong, W. L.; Boix, P. P.; Prabhakar, R. R.; Baikie, T.; Shi, C.; Ding, H.; Ramesh, R.; Asta, M.; Graetzel, M.; Mhaisalkar, S.G.; Mathews, N. Lead-Free Halide Perovskite Solar Cells with High Photocurrents Realized Through Vacancy Modulation. *Adv. Mater.* **2014**, 26 (41), 7122–7127.

(21) Koh, T. M.; Krishnamoorthy, T.; Yantara, N.; Shi, C.; Leong, W. L.; Boix, P. P.; Grimsdale, A. C.; Mhaisalkar, S. G.; Mathews, N. Formamidinium Tin-Based Perovskite with Low Eg for Photovoltaic Applications. *J. Mater. Chem. A* **2015**, 3

(29), 14996–15000.
(22) Marshall, K. P.; Walton, R. I.; Hatton, R. A. Tin Perovskite/Fullerene Planar Layer Photovoltaics: Improving the Efficiency and Stability of Lead-Free Devices. *J. Mater. Chem. A* **2015**, 3, 11631-11640.
(23) Lee, S. J.; Shin, S. S.; Kim, Y. C.; Kim, D.; Ahn, T. K.; Noh, J. H.; Seo, J.; Seok, S. I. Fabrication of Efficient Formamidinium Tin Iodide Perovskite Solar Cells through SnF(2)-Pyrazine Complex. *J. Am. Chem. Soc.* **2016**, 138, 3974-7.
(24) Chen, M.; Ju, M. G.; Garces, H. F.; Carl, A. D.; Ono, L. K.; Hawash, Z.; Zhang, Y.; Shen, T.; Qi, Y.; Grimm, R. L.; Pacifici, D.; Zeng, X. C.; Zhou, Y.; Padture, N. P. Highly Stable and Efficient All-Inorganic Lead-Free Perovskite Solar Cells with Native-Oxide Passivation. *Nat. Commun.* **2019**, 10 (16), 1-8.
(25) Ke, J. C.-R.; Lewis, D. J.; Walton, A. S.; Spencer, B. F.; O'Brien, P.; Thomas, A. G.; Flavell, W. R. Ambient-Air-Stable Inorganic Cs2SnI6 Double Perovskite Thin Films Via Aerosol-Assisted Chemical Vapour Deposition. *J. Mater. Chem. A* **2018**, 6, 11205-11214.
(26) Lee, B.; Stoumpos, C. C.; Zhou, N.; Hao, F.; Malliakas, C.; Yeh, C. Y.; Marks, T. J.; Kanatzidis, M. G.; Chang, R. P. Air-Stable Molecular Semiconducting Iodosalts for Solar Cell Applications: Cs2SnI6 as a Hole Conductor. *J. Am. Chem. Soc.* **2014**, 136, 15379-85.
(27) Shin, H.; Kim, B.-M.; Jang, T.; Kim, K. M.; Roh, D.-H.; Nam, J. S.; Kim, J. S.; Kim, U.-Y.; Lee, B.; Pang, Y.; Kwon, T.-H. Surface State-Mediated Charge Transfer of Cs2SnI6 and Its Application in Dye-Sensitized Solar Cells. *Adv. Energy Mater.* **2019**, 9 (3), 1803243.
(28) Kaltzoglou, A.; Antoniadou, M.; Kontos, A. G.; Stoumpos, C. C.; Perganti, D.; Siranidi, E.; Raptis, V.; Trohidou, K.; Psycharis, V.; Kanatzidis, M. G.; Falaras, P. Optical-Vibrational Properties of the Cs2SnX6 (X = Cl, Br, I) Defect Perovskites and Hole-Transport Efficiency in Dye-Sensitized Solar Cells. *J. Phys. Chem. C* **2016**, 120, 11777-11785.
(29) Chen, J.; Luo, Z.; Fu, Y.; Wang, X.; Czech, K. J.; Shen, S.; Guo, L.; Wright, J. C.; Pan, A.; Jin, S. Tin(IV)-Tolerant Vapor-Phase Growth and Photophysical Properties of Aligned Cesium Tin Halide Perovskite (CsSnX3; X = Br, I) Nanowires. *ACS Energy Lett.* **2019**, 4, 1045-1052.
(30) Chen, L. J.; Lee, C. R.; Chuang, Y. J.; Wu, Z. H.; Chen, C. Synthesis and Optical Properties of Lead-Free Cesium Tin Halide Perovskite Quantum Rods with High-Performance Solar Cell Application. *J. Phys. Chem. Lett.* **2016**, 7, 5028-5035.
(31) Guo, F.; Lu, Z.; Mohanty, D.; Wang, T.; Bhat, I. B.; Zhang, S.; Shi, S.; Washington, M. A.; Wang, G.-C.; Lu, T.-M. A Two-Step Dry Process for Cs2SnI6 Perovskite Thin Film. *Mater. Res. Lett.* **2017**, 5, 540-546.
(32) Saparov, B.; Sun, J.-P.; Meng, W.; Xiao, Z.; Duan, H.-S.; Gunawan, O.; Shin, D.; Hill, I. G.; Yan, Y.; Mitzi, D. B. Thin-Film Deposition and Characterization of a Sn-Deficient Perovskite Derivative Cs2SnI6. *Chem. Mater.* **2016**, 28, 2315-2322.
(33) Song, T.-B.; Yokoyama, T.; Aramaki, S.; Kanatzidis, M. G. Performance Enhancement of Lead-Free Tin-Based Perovskite Solar Cells with Reducing Atmosphere-Assisted Dispersible Additive. *ACS Energy Lett.* **2017**, 2, 897-903.
(34) Qiu, X.; Cao, B.; Yuan, S.; Chen, X.; Qiu, Z.; Jiang, Y.; Ye, Q.; Wang, H.; Zeng, H.; Liu, J.; Kanatzidis, M. G. From Unstable CsSnI3 to Air-Stable Cs2SnI6: A Lead-

Free Perovskite Solar Cell Light Absorber with Bandgap of 1.48 eV and High Absorption Coefficient. *Sol. Energy Mater. Sol. Cells* **2017**, 159, 227-234.

(35) Della Gaspera, E.; Peng, Y.; Hou, Q.; Spiccia, L.; Bach, U.; Jasieniak, J. J.; Cheng, Y.-B. Ultra-Thin High Efficiency Semitransparent Perovskite Solar Cells. *Nano Energy* **2015**, 13, 249-257.

(36) Masi, S.; Rizzo, A.; Munir, R.; Listorti, A.; Giuri, A.; Esposito Corcione, C.; Treat, N. D.; Gigli, G.; Amassian, A.; Stingelin, N.; Colella, S. Organic Gelators as Growth Control Agents for Stable and Reproducible Hybrid Perovskite-Based Solar Cells. *Adv. Energy Mater.* **2017**, 7, 1602600.

(37) Eperon, G. E.; Burlakov, V. M.; Goriely, A.; Snaith, H. J. Neutral Color Semitransparent Microstructured Perovskite Solar Cells. *ACS Nano* **2014**, 8, 591-598.

(38) Hecht, E.; Zając, A. Optics. Addison-Wesley Pub. Co.: **1974**.

(39) Phillips, L. J.; Rashed, A. M.; Treharne, R. E.; Kay, J.; Yates, P.; Mitrovic, I. Z.; Weerakkody, A.; Hall, S.; Durose, K. Dispersion Relation Data for Methylammonium Lead Triiodide Perovskite Deposited on a (100) Silicon Wafer Using a Two-Step Vapour-Phase Reaction Process. *Data in Brief* **2015**, 5, 926-928.

(40) Luque, A.; Hegedus, S. Handbook of Photovoltaic Science and Engineering, Wiley, **2003**.